Inorg. Chem. **2002**, *41*, 3705–3712

Temperature Dependence of the Crystal Lattice Organization of Coordination Compounds Involving Nitronyl Nitroxide Radicals: A Magnetic and Structural Investigation

Mohammed Fettouhi,*,† Bassam El Ali,† Abdel Moneim El-Ghanam,† Stéphane Golhen,‡ Lahcène Ouahab,*,‡ Nathalie Daro,§ and Jean-Pascal Sutter*,§

Chemistry Department, King Fahd University of Petroleum and Minerals, Dhahran 31261, Saudi Arabia, Laboratoire de Chimie du Solide et Inorganique Moléculaire, UMR 6511, Université de Rennes 1, Institut de Chimie de Rennes, Campus de Beaulieu, 35042 Rennes Cedex, France, and Groupe des Sciences Moléculaires, Institut de Chimie de la Matière Condensée de Bordeaux, UPR CNRS No. 9048, F-33608 Pessac, France

Received January 7, 2002

Four new mononuclear complexes of formula $Cd(PN)_4(NCS)_2$ (**A**), $Cd(PNN)_4(N_3)_2$ **(B)**, $Zn(PNN)_4(N_3)_2$ **(C),** and $Zn(PNN)_2(NCS)_2$ **(D)**, where PNN stands for 2-(4-pyridyl)-4,4,5,5-tetramethylimidazoline-1-oxyl-3-oxide and PN for 2-(4-pyridyl)-4,4,5,5-tetramethylimidazoline-1-oxyl, were synthesized and structurally and magnetically characterized. The X-ray structures of compounds **B** and **C** were also determined at 90 K. Compounds **A**–**C** crystallize in the triclinic space group $P\bar{1}$ (No. 2), and **D** crystallizes in the monoclinic space group $P2_1/m$ (No. 11). **A**–**C** adopt a centrosymmetric distorted octahedral geometry in which the metal ions are bonded to four radical ligands through the nitrogen atom of the pyridyl rings and the azido or thiocyanato ligands occupy the apical positions. Compound **D** adopts a distorted tetrahedral geometry in which the zinc ion is bonded to two radicals and two thiocyanato ligands. As suggested by their magnetic behavior, the low-temperature X-ray structures of **B** and **C** show that these compounds undergo a clear structural change with respect to the room-temperature structures. The experimental magnetic behaviors were perfectly reproduced by a dimer model for **A**–**C** and an alternating chain model for **D** while the sudden breaks observed in the $\chi_M T$ versus T curves for **B** and **C** were well accounted for by the high- and low-temperature X-ray structures. For all these complexes the crystal structures favor significant overlap between molecular magnetic orbitals leading to rather strong intermolecular antiferromagnetic interactions.

Introduction

The persistent organic radicals of the type aminoxyl have attracted much interest during the past decade because they have been envisaged as active building blocks for the construction of molecule-based magnetic materials. Among them the nitronyl nitroxide (i.e. 4,4,5,5-tetramethylimidazoline-1-oxyl-3-oxide) is certainly the most versatile. The exchange interactions between such neighboring organic open-shell molecules is usually understood by the mean of the McConnell theory which quite simply rationalizes the magnetic behavior through the short intermolecular distances between spin-bearing atoms.[1] A systematic magneto−structural correlation of a series of reported organic materials, however, revealed no statistically significant differences in the relative spatial disposition of the NO group (seat of the unpaired electron) with respect, for instance, to a neighboring NO group between compounds with either a dominant ferro- or antiferromagnetic behavior.[2]

As part of our ongoing study on the chemistry and magnetic properties of supramolecular open-shell architectures,[3−6] we envisaged the possibility of using preformed high-spin

* To whom correspondence should be addressed. E-mail: M.F., fettouhi@kfupm.edu.sa; L.O., ouahab@univ-rennes1.fr; J.-P.S., jpsutter@icmcb.u-bordeaux.fr.

† King Fahd University of Petroleum and Minerals.

‡ Université de Rennes 1.

§ Institut de Chimie de la Matière Condensée de Bordeaux.

(1) McConnel, H. M. *J. Chem. Phys.* **1963**, *39*, 1910.

(2) (a) Deumal, M.; Cirujeda, J.; Veciana, J.; Novoa, J. J. *Chem.—Eur. J.* **1999**, *5*, 1631−42. (b) A criticism of the McConnell theory can be found in the following: Deumal, M.; Novoa, J. J.; Bearpark, M. J.; Celani, P.; Olivucci, M.; Robb, M. A. *J. Phys. Chem. A* **1998**, *102*, 8404.

(3) Daro, N.; Sutter, J.-P.; Pink, M.; Kahn, O. *J. Chem. Soc., Perkin Trans. 2* **2000**, 1087−9.

10.1021/ic020021p CCC: $22.00
Published on Web 06/06/2002

Chart 1

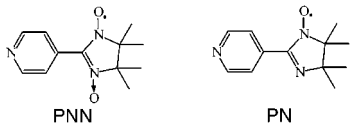

compounds as building blocks for the preparation of extended assemblies. Typical examples of such compounds consist in Mn(II) ions linked to an either two or four aminoxyl-substituted pyridine ligand. The intramolecular exchange interaction between the metal ions and the radical units being ferromagnetic, the ground states for these compounds are $S = 7/2$ and $9/2$ respectively for $[Mn(PNN)_2]^{2+}$ and $[Mn(PNN)_4]^{2+}$, where PNN stands for (nitronyl nitroxide)-4-pyridine[7,8] (see Chart 1). These building blocks can be assemble in systems of high nuclearity by the mean of bridging ligands such as pseudohalide anions. For instance, 1D and 2D networks have been obtained with dicyanamide or $[Ag(CN)_2]^-$ anions acting as bridging ligands.[9−11] A noticeable feature for these compounds observed for most of both the molecular building blocks and the extended structures is an anomaly in the plot $\chi_M T$ versus T of the temperature dependence of their molar magnetic susceptibility, χ_M. A more or less pronounced step is visible in the temperature domain 100−250 K. Such a sharp changing of the slop of the $\chi_M T$ curve is the signature of a sudden modification of the exchange interactions between magnetic centers which may result from significant changes in the crystal lattice organization. To gain some insight into the origin of this anomaly, we considered a series of derivatives consisting in a diamagnetic metal ion linked to the paramagnetic pyridine derivatives, i.e. $[Cd(PN)_4(NCS)_2]$ (**A**), $[Cd(PNN)_4(N_3)_2]$ (**B**), $[Zn(PNN)_4(N_3)_2]$ (**C**), and $[Zn(PNN)_2(NCS)_2]$ (**D**) (PN stands for the imino nitroxide substituted pyridine ligand). We report here the structural and magnetic studies performed on these compounds. For two of them, X-ray structure analyses have been performed at temperatures above and below the temperature of the anomaly on the $\chi_M T$ versus T curves revealing alteration of the crystal packing. Moreover, the temperature dependence of the lattice rearrangement could be nicely followed through the evolution of the magnetic properties.

Experimental Section

Syntheses. 2-(4-Pyridyl)-4,4,5,5-tetramethylimidazoline-1-oxyl-3-oxide (PNN) was prepared using a literature procedure.[12]

Compound A. To a solution of cadmium nitrate tetrahydrate (1 mmol) and PNN (4 mmol) in 50 mL of a 1:1 mixture of water−ethanol was added dropwise an aqueous solution of sodium thiocyanate (2 mmol). The mixture was stirred for 30 min and filtered. The green precipitate was collected, washed with water, and then ethanol and air-dried. Elemental analysis is consistent with the formula $Cd(PNN)_4(NCS)_2$. During the recrystallization process from dimethylformamide, the ligand is deoxygenated to the imino nitroxide radical, affording parallelopipedic dark brown crystals of formula $Cd(PN)_4(NCS)_2$. Anal. Obsd (calcd) for $CdN_{14}C_{50}H_{64}O_4S_2$: N, 17.81 (17.80); C, 54.43 (54.50); H, 6.05 (5.87); S, 5.44 (5.82). IR (KBr): 2026, 1614, 1540, 1448, 1414, 1404, 1372, 1326, 1296, 1156, 1136, 1064, 1014, 838, 660 cm^{-1}.

Compound B. To a solution of cadmium nitrate tetrahydrate (1 mmol) and PNN (4 mmol) in 50 mL of a 1:1 mixture of water−ethanol was added dropwise an aqueous solution of sodium azide (2 mmol). The mixture was stirred for 30 min and filtered. The filtrate was kept in the dark for 1 week to afford shiny black crystals.

Anal. Obsd (calcd) for $CdN_{18}C_{48}H_{64}O_8$: N, 21.88 (22.25); C, 50.67 (50.86); H, 5.68 (5.65). IR (KBr): 2038, 1604, 1548, 1458, 1400, 1374, 1320, 1216, 1168, 1138, 1062, 1010, 832, 654, 622, 542, 460 cm^{-1}.

Compound C. This compound was synthesized in a way similar to that for compound B, starting from zinc nitrate hexahydrate. Dark green crystals were hence obtained.

Anal. Obsd (calcd) for $ZnN_{18}C_{48}H_{64}O_8$: N, 23.22 (23.20); C, 52.18 (53.07); H, 6.07 (5.94). IR (KBr): 2054, 1604, 1548, 1454, 1396, 1374, 1320, 1214, 1168, 1138, 1066, 1008, 830, 652, 620, 542, 456 cm^{-1}.

Compound D. This compound was synthesized in a way similar to that for compound A, starting from zinc nitrate hexahydrate and PNN. Dark brown crystals were obtained from dimethylformamide.

Anal. Obsd (calcd) for $ZnN_8C_{26}H_{32}O_4S_2$: N, 17.28 (17.25); C, 47.98 (48.04); H, 4.98 (4.93); S, 9.27 (9.86). IR (KBr): 2090, 2062, 1618, 1546, 1450, 1408, 1378, 1318, 1214, 1168, 1134, 1068, 1030, 836, 662, 620, 542, 462 cm^{-1}.

Spectral and Magnetic Measurements. The IR spectra were measured on Perkin-Elmer spectrophotometer. Magnetic measurements were carried out using a Quantum Design SQUID MPMS-5S magnetometer working down to 2 K with magnetic fields up to 50 kOe. Data were corrected for the contribution of the sample holder, and diamagnetic contributions were estimated from Pascal's constants.

X-ray Data Collection and Structure Determination. Crystals were mounted on an glass fiber. Data collections at room temperature were performed on an Enraf-Nonius CAD4 diffractometer equipped with graphite-monochromatized Mo Kα radiation (λ = 0.710 73 Å). The unit cell parameters were obtained by least-squares fits of the automatically centered 25 reflections. Intensity data were corrected for Lorentz and polarization effects. Data reduction and absorption correction using the ψ-scan method were performed with MolEN programs.[13] Data collections for **B** and **C** at low temperature were performed on an Kappa CCD Enraf-Nonius diffractometer equipped with an Oxford cooling system. The slope of the temperature decrease was only 3 K/h to preserve the crystal quality. For all structural studies, structure solution and refinements were conducted with SHELXS-97 and SHELXL-97, respectively.[14,15] Crystallographic data are given in Table 1. Hydrogen atoms were included at calculated positions with isotropic thermal parameters

(4) Rancurel, C.; Leznoff, D. B.; Sutter, J.-P.; Guionneau, P.; Chasseau, D.; Kliava, J.; Kahn, O. *Inorg. Chem.* **2000**, *39*, 1602−5.
(5) Mortl, K. P.; Sutter, J.-P.; Golhen, S.; Ouahab, L.; Kahn, O. *Inorg. Chem.* **2000**, *39*, 1626−7.
(6) Ouahab, L. *Chem. Mater.* **1997**, *9*, 1909.
(7) Fettouhi, M.; Khaled, M.; Waheed, A.; Golhen, S.; Ouahab, L.; Sutter, J.-P.; Kahn, O. *Inorg. Chem.* **1999**, *38*, 3967−71.
(8) Caneschi, A.; Ferraro, F.; Gatteschi, D.; Rey, P.; Sessoli, R. *Inorg. Chem.* **1990**, *29*, 4217−23.
(9) Dasna, I.; Golhen, S.; Ouahab, L.; Peña, O.; Guillevic, J.; Fettouhi, M. *J. Chem. Soc., Dalton Trans.* **2000**, 129.
(10) Dasna, I.; Golhen, S.; Ouahab, L.; Pena, O.; Daro, N.; Sutter, J.-P. *C. R. Acad. Sci. Paris, Ser. IIc* **2001**, 125−33.
(11) Dasna, I.; Golhen, S.; Ouahab, L.; Daro, N.; Sutter, J.-P. *Polyhedron* **2001**, *20*, 1371−4.
(12) Ullman, E. F.; Call, L.; Osiecki, J. H. *J. Org. Chem.* **1970**, *35*, 3623−31.
(13) *(MolEN), C. S. A.*; Enraf-Nonius: Delft, The Netherlands, 1990.

Table 1. Crystallographic Data for **A**−**D**

		B		C		
	A	293 K	90 K	293 K	90 K	**D**
formula	$CdC_{50}H_{64}N_{14}O_4S_2$	$CdC_{48}H_{64}N_{18}O_8$	$CdC_{48}H_{64}N_{18}O_8$	$ZnC_{48}H_{64}N_{18}O_8$	$ZnC_{48}H_{64}N_{18}O_8$	$ZnC_{26}H_{32}N_8O_4S_2$
fw	1101.67	1133.57	1133.57	1086.54	1086.54	650.09
cryst syst	triclinic	triclinic	triclinic	triclinic	triclinic	monoclinic
space group	$P\bar{1}$	$P\bar{1}$	$P\bar{1}$	$P\bar{1}$	$P\bar{1}$	$P2_1/m$
T (K)	293(2)	293(2)	90(2)	293(2)	90(2)	293(2)
λ (Å)	0.710 73	0.710 73	0.710 73	0.710 73	0.710 73	0.710 73
ρ_{calc} (g·cm^{-3})	1.317	1.382	1.414	1.343	1.387	1.343
μ (mm^{-1})	0.521	0.469	0.480	0.526	0.543	1.000
a (Å)	7.3016(12)	7.209(2)	7.1420(3)	7.171(3)	7.0908(5)	6.191(4)
b (Å)	13.744(3)	13.802(3)	13.4923(6)	13.7915(16)	13.4442(10)	20.361(3)
c (Å)	14.2278(12)	14.009(4)	14.1634(7)	13.967(4)	14.0037(10)	12.048(6)
α (deg)	91.3115(13)	90.34(2)	90.824(2)	90.150(16)	90.6470(4)	90
β (deg)	99.581(9)	102.18(2)	101.843(2)	103.22(3)	101.9960(5)	97.36(2)
γ (deg)	97.721(19)	91.26(2)	94.503(2)	91.931(18)	94.8480(3)	90
V (Å^3)	1393.6(4)	1362.1(7)	1330.99(10)	1343.8(7)	1300.58(16)	1506.1(11)
Z	1	1	1	1	1	2
R ($I_{obs} > 2\sigma(I)$)[a]	0.0601 (4505)	0.0335 (4701)	0.0522 (4132)	0.0442 (3365)	0.0626 (4252)	0.0592 (2001)
wR2[b]	0.1626	0.0798	0.1038	0.0955	0.1557	0.1494

[a] $R = \sum||F_o| - |F_c||/\sum|F_o|$. [b] $wR2 = \{\sum[w(F_o^2 - F_c^2)^2]/\sum[w(F_o^2)^2]\}^{1/2}$.

Table 2. Selected Bond Lengths (Å) and Bond Angles (deg) for **A**−**D**

			B			C			
	A		293	90		293	90		**D**
Cd−N7	2.312(4)	Cd−N7	2.278(2)	2.314(3)	Zn−N7	2.086(2)	2.086(3)	Zn−N5	1.949(6)
Cd−N1	2.384(4)	Cd−N1	2.392(2)	2.387(3)	Zn−N1	2.249(2)	2.254(3)	Zn−N2	1.955(6)
Cd−N4	2.396(4)	Cd−N4	2.419(2)	2.401(3)	Zn−N4	2.257(2)	2.265(3)	Zn−N1	2.038(3)
N1−C5	1.317(7)	N7−N8	1.169(3)	1.202(4)	N7−N8	1.186(3)	2.201(4)	N1−C5	1.334(5)
N1−C1	1.321(6)	N8−N9	1.153(3)	1.181(4)	N8−N9	1.150(3)	1.159(4)	N1−C1	1.338(5)
N2−O1	1.277(6)	N1−C5	1.335(3)	1.362(5)	N1−C1	1.340(3)	1.344(4)	N3−O1	1.259(4)
N2−C6	1.378(7)	N1−C1	1.342(3)	1.338(5)	N1−C5	1.342(4)	1.334(4)	N3−C6	1.342(5)
N2−C7	1.482(7)	N2−O2	1.279(3)	1.288(4)	N2−O2	1.274(3)	1.282(3)	N3−C8	1.495(5)
N3−C6	1.303(6)	N2−C6	1.338(3)	1.376(5)	N2−C6	1.351(4)	1.336(4)	N4−C6	1.352(5)
N3−C8	1.495(7)	N2−C7	1.501(3)	1.481(5)	N2−C7	1.508(3)	1.501(4)	N4−C7	1.492(5)
N4−C13	1.317(7)	N3−O1	1.268(3)	1.311(4)	N3−O1	1.272(3)	1.284(3)	N4−O2	1.271(4)
N4−C17	1.324(7)	N3−C6	1.349(3)	1.351(5)	N3−C6	1.347(3)	1.351(4)		
N5−O3	1.272(7)	N3−C8	1.488(3)	1.510(5)	N3−C8	1.499(4)	1.510(4)		
N5−C18	1.374(7)	N4−C13	1.328(3)	1.341(5)	N4−C13	1.338(4)	1.369(4)		
N5−C20	1.481(7)	N4−C17	1.333(3)	1.370(4)	N4−C17	1.340(3)	1.338(4)		
N6−C18	1.296(7)	N5−O(3)	1.280(3)	1.288(4)	N5−O3	1.278(3)	1.272(4)		
N6−C19	1.490(8)	N5−C18	1.348(3)	1.388(4)	N5−C18	1.344(3)	1.369(4)		
		N5−C19	1.508(3)	1.493(5)	N5−C19	1.508(4)	1.501(4)		
		N6−O4	1.279(3)	1.318(4)	N6−O4	1.272(3)	1.284(3)		
		N6−C18	1.349(3)	1.346(5)	N6−C18	1.347(4)	1.341(4)		
		N6−C20	1.510(3)	1.525(5)	N6−C20	1.496(4)	1.518(4)		
N7−Cd− N1	89.97(15)	N7−Cd− N4	87.56(8)	89.91(11)	N7−Zn− N1	87.32(9)	87.04(11)	N5−Zn− N2	117.0(3)
N7−Cd− N4	88.52(14)	N7−Cd− N1	88.17(8)	87.94(11)	N7−Zn− N4	87.99(9)	89.69(10)	N5−Zn− N1	106.40(14)
N1−Cd− N4	89.15(14)	N4−Cd− N1	91.60(7)	93.58(11)	N1−Zn− N4	91.79(8)	92.88(11)	N2−Zn− N1	111.72(14)

proportional to those of the connected atoms. Selected bond lengths and angles are given in Table 2. Complete bond lengths and bond angles, anisotropic thermal parameters, and calculated hydrogen coordinates are deposited as Supporting Information. Figures 1, 3, and 6 give, at room temperature, the ORTEP atomic labeling schemes for compounds **A**, **B,** and **D**, respectively, compounds **B** and **C** being isostructural.

Results

Crystal Structures. The molecular structure of compound **A**, $Cd(PN)_4(NCS)_2$, with the labeling scheme is shown in Figure 1; the crystal structure is displayed in Figure 2 as a projection in the *bc* plane. The Cd(II) ion is bonded to four nitrogen atoms of the pyridyl groups in addition to two nitrogen atoms of the thiocyanate ligands, occupying the apical positions. It lies on an inversion center and adopts an octahedral coordination with N−Cd−N angles in the range 88.52(14)−89.97(15)°. The NCS unit (177.6(6)°) forms an angle of 135.9(4)° with the Cd−N7 bond. The Cd−N(NCS) bond distance is 2.312(4) Å whereas the average Cd−N(pyridyl) bond distance is 2.390(4) Å. The dihedral angles between the N−C−NO moieties and the pyridyl rings for the two independent PN ligands are 22.6(4) and 19.2(3)°, whereas the dihedral angle between the two adjacent N−C−NO moieties of an asymmetric fragment is 67.0(1)°. The shortest intermolecular contact observed between two nitronyl nitroxide moieties takes place between the centrosymmetric oxygen atoms of the NO group (O1···O1 = 3.87(1) Å).

(14) Sheldrick, G. M. *SHELXS-97: Program for the solution of crystal structures*; University of Göttingen: Göttingen, Germany, 1997.

(15) Sheldrick, G. M. *Program for the refinement of crystal structures*; University of Göttingen: Göttingen, Germany, 1997.

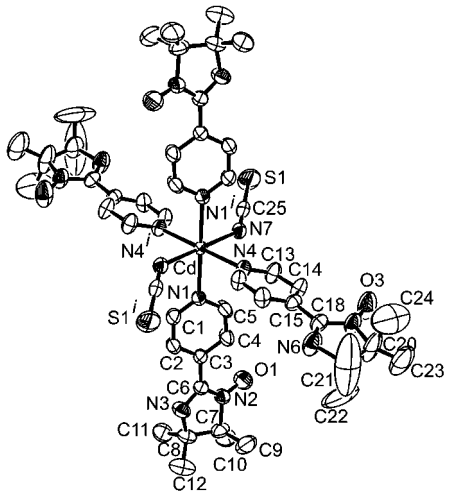

Figure 1. ORTEP view of the molecular structure of **A.** Thermal ellipsoids are drawn at the 50% probability level.

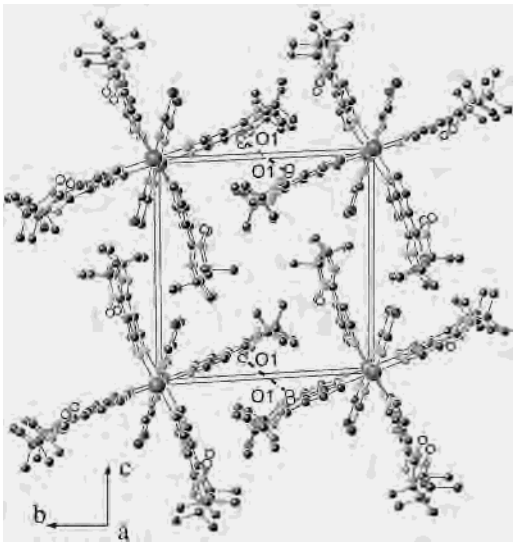

Figure 2. View of the structure of **A** in the *bc* plane. Selected intermolecular distances (Å): O1···O1^{i}, 3.87(1); O1···N2^{i}, 3.858(7); N2···N2^{i}, 4.247(9). i: $1 - x, -1 - y, -z$.

The structures of compounds **B**, $Cd(PNN)_4(N_3)_2$, and **C**, $Zn(PNN)_4(N_3)_2$, were studied both at 293 and 90 K. They are isostructural with the previously reported $Mn(PNN)_4(N_3)_2$.[7] The molecular structure of compound **B** with its labeling scheme is depicted in Figure 3, and the bond distances and bond angles at 293 and 90 K for **B** and **C** are given in Table 2. The metal ion lies on an inversion center and adopts a distorted octahedral coordination. It is bonded to four nitrogen atoms of the pyridyl groups in addition to two azido ligands occupying the apical positions. The M−N7(azido) bond distances are 2.278(2) [2.314(3) Å] (the value given in brackets refers to the data at 90 K) and 2.086(2) Å [2.086(3)°], and the N8−N7−M angles are 124.6(2)° [124.8(3)°] and 127.7(2)° [126.4(2)°] for **B** and **C**, respectively. The average M−N(pyridyl) bond distances are 2.405(2) Å [2.394(3) Å] for **B** and 2.253(2) Å [2.259(3) Å] for **C**. The dihedral angles between the ON−C−NO moieties and the pyridyl rings for the two independent PNN ligands are 27.4(2)° [30.6(3)°] and 34.2(2)° [29.2(2)°] for **B** and 27.2-

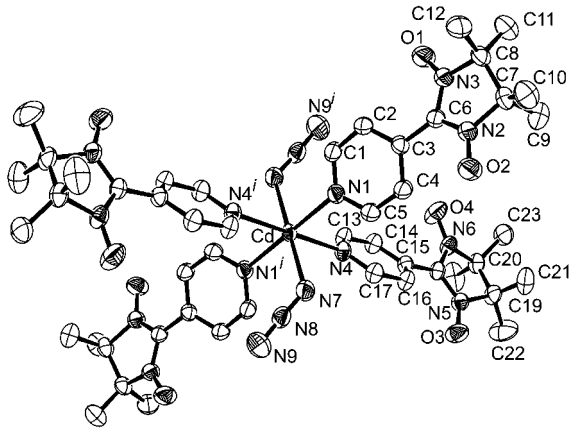

Figure 3. ORTEP view of the molecular structure of **B.** Thermal ellipsoids are drawn at the 50% probability level.

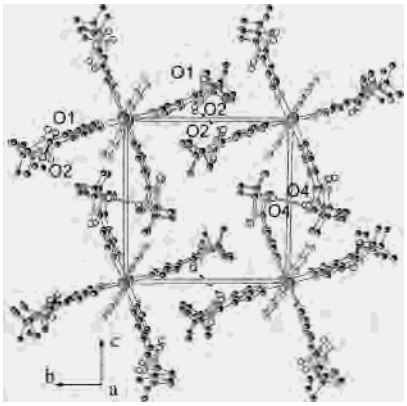

Figure 4. View of the structure of **B**, at room temperature, in the *bc* plane. Selected intermolecular distances (Å): O2···O2^{i}, 3.622(4); O4···O4^{ii}, 3.516(6); O2···N2^{i}, 3.558(3); O4···N6^{ii}, 3.526(4); N2···N2^{i}, 3.935(4); N6···N6^{ii}, 3.971(5). N−O/N−O dihedral angle: 23(1)° for both ON−C−NO moieties. Data for compound **C** (Å): O2···O2^{i}, 3.690(5); O4···O4^{ii}, 3.532(6); O2···N2^{i}, 3.622(4); O4···N6^{ii}, 3.545(4); N2···N2^{i}, 3.984(5); N6···N6^{ii}, 3.987(5). N−O/N−O dihedral angle: 21.5(11) and 22.5(11)° for O2−N2−N3−O1 and O4−N6−N5−O3, respectively. i: $1 - x, -1 - y, -z$. ii: $1 - x, -y, 1 - z$.

(2)° [31.8(3)] and 35.0(2)° [28.2(2)] for **C** while those between the two adjacent ON−C−NO moieties of an asymmetric fragment are 73.7(2)° [73.1(3)°] and 74.8(2)° [72.3(3)°] for compounds **B** and **C**, respectively. The crystal structure of **B** at 293 K is displayed in Figure 4 as a projection on the *bc* plane. For this temperature, the shortest intermolecular contacts are established between oxygen atoms of the NO groups with distances of 3.516(6) and 3.622(5) Å respectively for O4···O4 and O2···O2. This contact scheme develops in a 2D array parallel to the *bc* plane. A view of the relative positions of two neighboring nitronyl nitroxide moieties belonging to adjacent complexes is shown in Figure 5. Geometrical parameters relevant for the magnetic interactions resulting from these contacts are depicted Figure 5. The values of these parameters are given in Tables 3 and 4 for **A** and **B**, respectively.[16]

The low-temperature cell parameters for both derivatives are characterized by significant decrease of parameter *b*

(16) Cogne, A.; Laugier, J.; Luneau, D.; Rey, P. *Inorg. Chem.* **2000**, *39*, 5510.

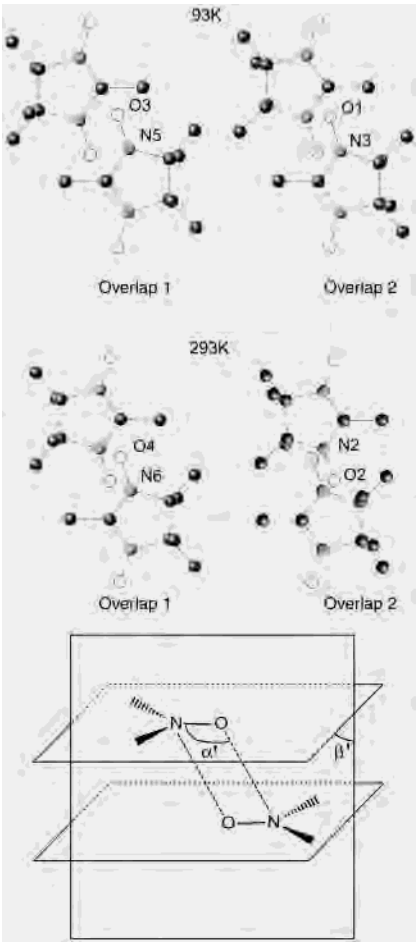

Figure 5. Details of the relative disposition of neighboring nitronyl nitroxide moieties in **B** [and **C**] at 293 and 90 K (values in Å). 293 K: O4···O4^{ii}, 3.516(6) [3.532(6)]; O4···N6^{ii}, 3.526(4) [3.545(4)]; O2···O2^{i}, 3.622(5) [3.690(5)]; N2···O2^{i}, 3.558(4) [3.622(4)]. 90 K: O3···O3^{iii}, 3.706(5) [3.742(5)]; O3···N5^{iii}, 3.610(4) [3.628(4)]; O1···O1^{iv}, 3.403(6) [3.389(5)]; O1···N3^{iv}, 3.313(4) [3.301(4)]. i: $1-x, -1-y, -z$. ii: $1-x, -y, 1-z$. iii: $-x, -y, -1-z$. iv: $-1-x, -1-y, -z$. The geometrical parameters α' and β' relevant for the magnetic interactions resulting from these contacts are also shown.

Table 3. Geometrical Parameters Relevant to the Magnetic Interactions in **B**

	overlap 1		overlap 2	
T (K)	293	90	293	90
α' (deg)	100.88(16)	90.75(18)	97.47(15)	97.36(20)
β' (deg)	79.3(2)	71.11(32)	87.4(2)	73.17(26)
O···O (Å)	3.516(6)	3.706(5)	3.622(5)	3.403(6)
O···N (Å)	3.526(4)	3.610(4)	3.558(4)	3.313(4)

Table 4. Geometrical Parameters Relevant to the Magnetic Interactions in **C**

	overlap 1		overlap 2	
T (K)	293	90	293	90
α' (deg)	100.92(18)	94.82(19)	97.03(17)	97.20(17)
β' (deg)	82.2(2)	74.50(29)	83.8(2)	73.25(22)
O···O (Å)	3.532(6)	3.742(5)	3.690(3)	3.389(5)
O···N (Å)	3.5445(4)	3.628(4)	3.622(4)	3.301(4)

(−2.2% for **B** and −2.5% for **C**) and increase of γ (+3.6% for **B** and +2.7% for **C**). The overall low-temperature crystal structures of **B** and **C** at first glance are very similar to the ones found at 293 K. Nevertheless, the intermolecular arrangements of the radical units reveals subtle differences. Indeed, by decrease of the temperature the overlapping NO moieties slide apart (overlap 1) and the β' parameter, defined in Figure 5, deviates significantly from 90° especially for the pair depicted in overlap 2.

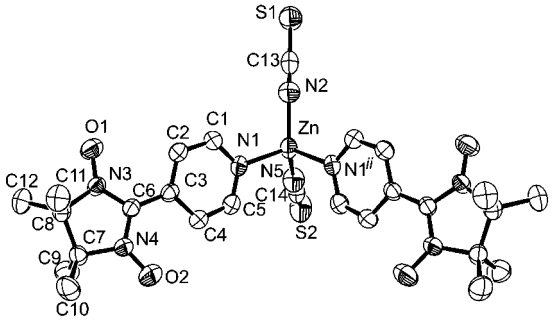

Figure 6. ORTEP view of the molecular structure of **D.** Thermal ellipsoids are drawn at the 50% probability level.

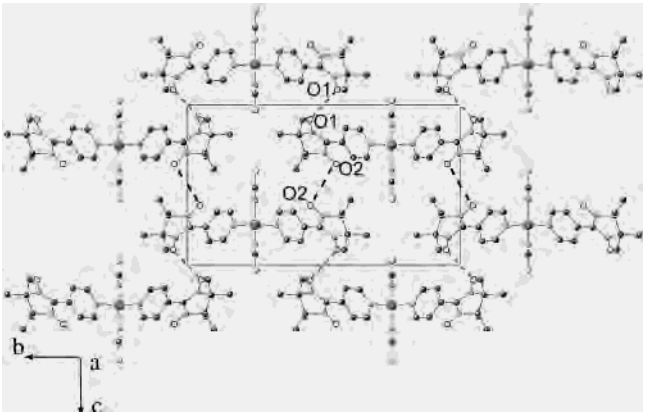

Figure 7. View of the structure of **D** in the *bc* plane. Selected intermolecular distances (Å): O1···O1^{iii}, 3.560(6); O2···O2^{iv}, 3.746(8); O1···N3^{iii}, 4.542(5); O2···N4^{iv}, 4.243(5). N−O/N−O dihedral angle: 15.1(17)°. iii: $2-x, 1-y, 2-z$. iv: $3-x, 1-y, 1-z$.

The molecular structure of compound **D** is displayed in Figure 6. The distorted tetrahedral coordination sphere is formed by two PNN and two thiocyanate ligands. The zinc ion and the two thiocyanate ligands are located on a mirror plane. The Zn−N1(pyridyl) bond distance is 2.038(3) Å, and the average Zn−NCS bond is 1.952(6) Å, with N−Zn−N angles in the range 106.4(1)−117.0(3)°. The dihedral angle between the ON−C−NO moiety and the pyridyl ring is 21.7-(4)°, and the dihedral angle between the two pyridyl rings is 76.0(1)°. The crystal structure is shown in Figure 7 as a projection in the *bc* plane. As for compounds **B** and **C**, the shortest intermolecular distances are observed between oxygen atoms belonging to two adjacent radical moieties (O1···O1 = 3.560(6) Å and O2···O2 = 3.746(8) Å).

Magnetic Properties. In compounds **A**−**D**, diamagnetic metal centers have been used as a platform for the construction of molecules in which the spin carriers are located not at the metal center but around the periphery. The temperature dependencies of the magnetic susceptibility for these compounds were investigated in the temperature range 2−300 K, with an applied field of 1000 Oe. The plots of $\chi_M T$ versus *T*, where χ_M stands for the molar magnetic susceptibility and *T* for the temperature, are depicted in Figures 8−11,

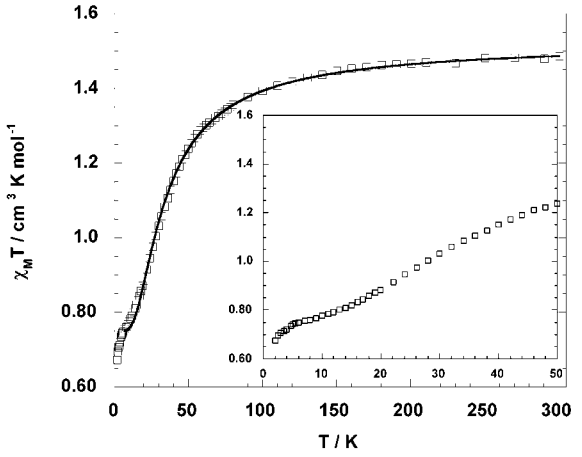

Figure 8. Experimental and calculated (—) $\chi_M T$ versus T curve for compound **A**. The inset is an expanded view of the low-temperature domain.

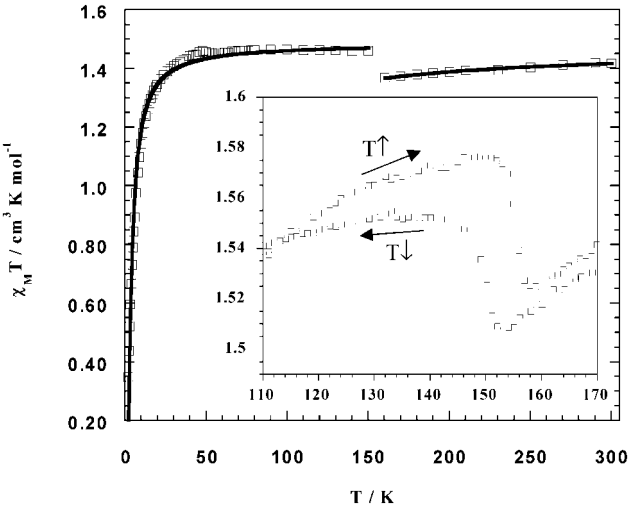

Figure 9. Experimental and calculated (—) $\chi_M T$ versus T curve for compound **B**. The inset highlights the behavior in the cooling ($T\downarrow$) and warming ($T\uparrow$) mode.

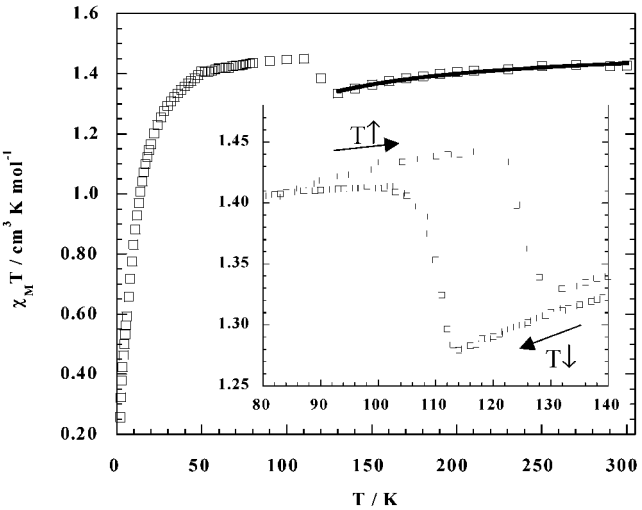

Figure 10. Experimental and calculated (—) $\chi_M T$ versus T curve for compound **C**. The inset highlights the behavior in the cooling ($T\downarrow$) and warming ($T\uparrow$) mode.

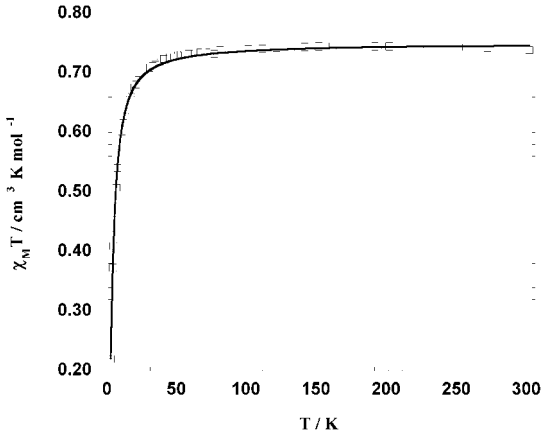

Figure 11. Experimental and calculated (—) $\chi_M T$ versus T curve for compound **D**.

respectively for compounds **A**−**D**. As a general trend, the solid-state magnetic behavior is governed by overall antiferromagnetic interactions. At high temperatures $\chi_M T$ correspond to the expected values for the four and two noncorrelated $S = 1/2$ spins for **A**−**C** and **D**, respectively, and as the temperature is lowered to 2 K, the $\chi_M T$ values decrease. Closer examination of Figures 8−11, however, reveals peculiar features.

For $Cd(PN)_4(NCS)_2$ (**A**) (Figure 8) the $\chi_M T$ value steadily decreases as the temperature is lowered from 300 to ca. 15 K to tend to a plateau value of 0.75 cm^3 K mol^{-1} (insert Figure 8); below 5 K $\chi_M T$ further decreases. The observation of this plateau indicates that the magnetic behavior observed in the 300−15 K range concerns only two of the spin carriers of the molecule. These are involved in substantial antiferromagnetic interactions leading to the canceling of their magnetic moment. Such a behavior is not consistent with intramolecular exchange interaction between the spin carriers. Indeed, in compound **A** the four paramagnetic ligands are equivalent and an intramolecular interaction should involve all of them. Diamagnetic metal ions have been shown to transmit magnetic interactions between aminoxyl radicals, but substantial interactions have been observed only when the aminoxyl units were directly coordinated to the metal ion.[17−19] Such a superexchange type interaction does not apply for compound **A**. Moreover, the magnetic interaction between the nitronyl nitroxide radical and a paramagnetic metal through the *para*-pyridine linker has been shown to be rather weak.[7,20] Consequently, for **A** an intramolecular radical−radical interaction via the metal center should be very weak, if any.

The magnetic behavior observed for compound **A** can be understood by considering the results of the X-ray structure analysis. For two imino nitroxide units of a molecule, the radical-containing aminoxyl fragments have been found in close contact with the N−O of a neighboring radical unit with a O···O separations of 3.87 Å, whereas for the two remaining radicals such a pair type association does not exist.

(17) Oshio, H.; Ohto, A.; Ito, T. *Chem. Commun.* **1996**, 1541.
(18) Oshio, H.; Watanabe, T.; Ohto, A.; Ito, T.; Ikoma, T.; Tero-Kubota, S. *Inorg. Chem.* **1997**, *36*, 3014−21.
(19) Sutter, J.-P.; Kahn, M. L.; Golhen, S.; Ouahab, L.; Kahn, O. *Chem.—Eur. J.* **1998**, *4*, 571−6.
(20) Caneschi, A.; Gatteschi, D.; Rey, P. *Prog. Inorg. Chem.* **1991**, *39*, 331.

The experimental magnetic behavior between 300 and 5 K could be perfectly reproduced by a dimer model. The interaction parameter was then found as $J = -42.4 \pm 0.3$ cm^{-1} ($H = -J\mathbf{S}_1\cdot\mathbf{S}_2$).[21] This substantial antiferromagnetic interaction parameter is indicative of a favorable overlap of groups bearing a high spin density, i.e. the N−O moieties. Strong exchange interactions between proximate aminoxyl radicals have been found previously.[22−27] The magnetic behavior below 10 K is the result of much weaker antiferromagnetic interaction involving the two remaining radicals.

The magnetic behavior of $Cd(PNN)_4(N_3)_2$ (**B**) and the corresponding Zn(II) compound (**C**) are characterized by a breaking in the $\chi_M T$ versus T curves. For compound **B** (Figure 9) the $\chi_M T$ value recorded in the warming mode decreases from 1.41 to 1.37 cm^3 K mol^{-1} while the temperature is lowered from 300 to 160 K. At this temperature, a steep increase of the $\chi_M T$ is observed, reaching a value of 1.46 cm^3 K mol^{-1} at 150 K. Below this temperature it remains constant down to ca. 50 K where it decreases again. For compound **C** this break in the $\chi_M T$ versus T curve is even more pronounced (Figure 10). At 130 K, the $\chi_M T$ value for **C** has decreased to 1.33 cm^3 K mol^{-1}, and over a 20 K domain, it increases again to reach 1.45 cm^3 K mol^{-1} at 110 K, the behavior for lower temperatures being then the same as for **B**.

The crystal structure analyses for these compounds performed above and below the temperature range of the magnetic anomalies indicate that each radical unit of a molecule is packed in such a way that it forms a pair with a nitronyl nitroxide group belonging to a neighboring molecule. For this reason, to get some insight into the magnetic behavior of these compounds, we analyzed the magnetic data for **B** and **C** by a dimer model. For compound **B**, the experimental curves in both the high (160−300 K) and low (2−150 K) temperature range are well reproduced by the model suggesting that the dominant antiferromagnetic interaction occurs between pairs of radicals (Figure 9). As expected, however, dramatic differences in the exchange parameters were found. For the high-temperature domain the best fit yielded $J_{HT} = -30 \pm 1$ cm^3 K mol^{-1} whereas for the low-temperature the exchange parameter was found as $J_{LT} = -4.8 \pm 0.1$ cm^3 K mol^{-1}. For compound **C**, only the high-temperature part could be reproduced by the dimer model; the interaction parameter was found as $J = -35.1 \pm 0.4$ cm^3 K mol^{-1} (Figure 10).

The temperature dependence of $\chi_M T$ for **B** and **C** compounds was recorded in the cooling and warming mode revealing the occurrence of a domain of bistabilty for the lattice organizations. For the Cd derivative, **B**, the step in the $\chi_M T$ curve is observed at 152 K in the cooling mode whereas in the warming mode the high-temperature lattice organization is recovered for 157 K (inset of Figure 9). For the Zn derivative, **C**, the temperature hysteresis reveals an even larger bistability domain. In the cooling mode, the transition from the high- to the low-temperature lattice is found at 114 K, and in the heating mode, the high-temperature organization is observed above 131 K (inset of Figure 10).

For compound **D** the intermolecular close contacts involving the radical-containing fragments lead to 1D arrays of spin carriers. Considering the nonequivalent and alternating NO···NO separations (3.566 and 3.746 Å), the magnetic behavior of compound **D** has been analyzed with an alternating chain model ($H = -J\Sigma_{i=1}^{n/2}[\mathbf{S}_{A_{2i}}\cdot\mathbf{S}_{A_{2i-1}} + \alpha\mathbf{S}_{A_{2i}}\cdot\mathbf{S}_{A_{2i+1}}]$).[21] The experimental $\chi_M T$ versus T curve (Figure 11) could be perfectly reproduced leading to the exchange parameters $J = -2.9 \pm 0.1$ cm^3 K mol^{-1} and $\alpha = 0.85$ ($\alpha J = -2.5 \pm 0.2$ cm^3 K mol^{-1}).

Discussion

The results gathered in this study reveal that differences in the crystal lattice organization could exist for molecule-based compounds between room and low temperature which may have dramatic effects on the bulk magnetic properties. The X-ray structure analyses performed at 293 and 90 K for compounds **C** and **D** show that the reorganization does not affect the integrity of the molecular fragment but the short distances existing between neighboring molecules. These involve the spin-bearing aminoxyl units, and consequently, a substantial effect on the magnetic behavior for the compounds is found. Interestingly for these compounds, the high-temperature lattice organization leads to strong antiferromagnetic interactions between the proximate spin carriers, with exchange parameters of $J_{HT} = -30$ and -35 cm^{-1} respectively for **B** and **C**, whereas the low-temperature organization leads to much weaker exchange interactions, $J_{LT} = -4.8$ cm^{-1} for **B**. Consequently, the evolution of the lattice organization becomes visible and can be followed by the means of the magnetic properties as depicted Figures 9 and 10. For both compounds, the passing over from one stage to the other is rather abrupt and a domain of bistability is revealed from temperature cycling experiments. A related behavior has been reported recently for an organic biradical derivative.[28]

For compounds **A**−**D** a diamagnetic metal center has been used to anchor the paramagnetic ligands. The metal ion thus controls the geometry of the molecule and may influence the inter- and intramolecular interactions of the periphery.[29−31] The magnetic properties for these compounds show that

(21) Kahn, O. *Molecular Magnetism*; VCH: Weinheim, Germany, 1993.
(22) Daro, N.; Guionneau, P.; Golhen, S.; Chasseau, D.; Ouahab, L.; Sutter, J.-P. *Inorg. Chim. Acta* **2001**, *326*, 47−52.
(23) Fujita, W.; Awaga, K. *Science* **1999**, *286*, 261−2.
(24) Akabane, R.; Tanaka, M.; Matsuo, K.; Koga, N.; Matsuda, K.; Iwamura, H. *J. Org. Chem.* **1997**, *62*, 8854.
(25) Awaga, K.; Yamagushi, A.; Oki, T. *Mol. Cryst. Liq. Cryst.* **1995**, *271*, 97.
(26) Ueda, K.; Tsujii, M.; Suga, T.; Sugimoto, T.; Kanehisa, N.; Kai, Y.; Hosoito, N. *Chem. Phys. Lett.* **1996**, *253*, 355.
(27) Lanfranc de Panthou, F.; Luneau, D.; Laugier, J.; Rey, P. *J. Am. Chem. Soc.* **1993**, *115*, 9095.
(28) Shultz, D. A.; Fico, R. M.; Boyle, P. D.; Kampf, J. W. *J. Am. Chem. Soc.* **2001**, *123*, 10403−4.
(29) Rancurel, C.; Sutter, J.-P.; Le Hoerff, T.; Ouahab, L.; Kahn, O. *New J. Chem.* **1998**, 1333−5.
(30) Leznoff, D. B.; Rancurel, C.; Sutter, J.-P.; Golhen, S.; Ouahab, S.; Rettig, S. J.; Kahn, O. *Mol. Cryst. Liq. Cryst.* **1999**, *334*, 425−36.
(31) Leznoff, D. B.; Rancurel, C.; Sutter, J.-P.; Rettig, S. J.; Pink, M.; Paulsen, C.; Kahn, O. *J. Chem. Soc., Dalton Trans.* **1999**, 3593−9.

neither the Cd(II) nor the Zn(II) ions mediate intramolecular exchange interactions between the paramagnetic ligands. The observed antiferromagnetic interactions are due to intermolecular interactions; the favorable overlap of the N−O groups containing high positive spin density provides a dominant mechanism for antiferromagnetic coupling.

A tentative correlation of the magnetic properties of compounds **A**−**D** with their crystal structure features can by proposed. We will consider the case of compound **B** as an illustrative example. The magnitude of the exchange interaction between aminoxyl units relies on their proximity and on the relative orientation of their π*-orbitals where the unpaired electron is located. A good estimation for the latter is provided by the geometrical parameters α' and β' defined in Figure 5. For compound **B** at 293 K the relevant parameters for two neighboring NO groups, i.e. the N···O distances of 3.526(4) and 3.558(4) Å, $\alpha' = 100.9$ and 97.5°, and $\beta' = 79.3$ and 87.4° (Table 3), are indicative of close and nearly superposed groups with the π*-orbitals pointing toward each other (β' close to 90°). This arrangement suggest a good overlap of the singly occupied molecular orbitals and should lead to significant antiferromagnetic interaction between the spin carriers. This is indeed confirmed by the exchange parameter, $J_{HT} = -30$ cm^{-1}, found for the high-temperature (300−160 K) behavior for compound **B**. For temperatures below the lattice reorganization, the relevant geometric parameters indicate a shortening of one N···O distance (overlap 2) but, more importantly, a significant decrease of β' (71.1 and 73.1°) which significantly deviates from 90°. Consequently, the π*-orbitals are tilted and their overlap is smaller than for the high-temperature situation. On that account, a weak exchange interaction is anticipated. This is exactly what has been found for the magnetic behavior for compound **B** in the 2−150 K temperature domain with an exchange parameter $J_{LT} = -4.8$ cm^{-1}. The same analyses hold for compound **C**. For compound **A** no evidence for a lattice reorganization becomes apparent from the magnetic behavior and the exchange parameters found, $J = -42.4$ cm^{-1}, is in line with the structural features at 293 K. A structural evolution as for compounds **B** and **C** should have been detected because of the rather strong antiferromagnetic interaction existing in **A**. For compound **D** at 293 K, the intermolecular distances involving the aminoxyl units, i.e., O1···O1′ (3.560(6) Å), O1···N3′ (4.542(5) Å), O2···O2′ (3.746(8) Å), and O2···N4′ (4.243(5) Å), suggest a much less significant overlap of the π*-orbitals. This is in line with the weaker interaction parameters, $J = -2.9$ and -2.5 cm^{-1}, determined for this compound. As for compound **A**, no evidence for a structural modification at low temperature is detected in the magnetic behavior of **D**. We may stress however that on the basis of the magnetic behavior alone a structural rearrangement cannot be excluded. Indeed, if a reorganization leads to a low-temperature situation for which the exchange will be of the same sign and magnitude as for the one for the high-temperature organization, the difference might be too small to be detected. Or even it may take place in the Curie domain and be unrevealed. This latter case may then lead to misleading magneto−structural correlation. The lack of cohesion and clear trends for organic materials pointed by a recent study[2] might at least partly result from the assumption that the crystal structures determined at room temperature remain the same for cryogenic temperatures where the magnetic features are revealed. Our results show that this is not always the case.

In compounds **A**−**D** the magnetic behavior originates exclusively from intermolecular exchange interaction between the organic spin carriers. As found for **A**−**C**, these antiferromagnetic interactions are rather strong, at least before the structural reorganization that occurs for the two **B** and **C** compounds at low temperature. These results lead to a better understanding of a result obtained previously for an isomorphous Mn(II) compound, $Mn(PN)_4(N_3)_2$.[7] For the latter (compound **C** in ref 7), a peculiar magnetic behavior was observed, in the temperature range 300−50 K, where the $\chi_M T$ value decreases, which clearly indicates substantial antiferromagnetic interactions. However, for temperatures below 50 K, $\chi_M T$ suddenly increases, the sign now for dominant ferromagnetic interactions. Such a behavior was rather puzzling. In light of the behavior we found for the related Cd, **B**, and Zn, **C**, derivatives, the magnetic behavior of the Mn(II) compound can be analyzed as follows. In the high-temperature domain, strong intermolecular antiferromagnetic interactions between the radical units are observed. Indeed, as for the Cd or Zn compounds, short intermolecular distances involving the aminoxyl N−O groups exist in the Mn derivative. These intermolecular interactions are much stronger than the intramolecular ferromagnetic Mn−radical interactions. However, as observed for **B** and **C**, for lower temperatures a structural reorganization probably occurs which dramatically decreases the intermolecular exchange interaction. The ferromagnetic interactions are then the dominant interactions, and as a consequence, $\chi_M T$ increases as the temperature is further lowered.

Concluding Remarks. The structural and magnetic studies performed on a series of coordination compounds composed of a diamagnetic metal ion and aminoxyl-substituted pyridine ligands permit one to highlight subtle crystal lattice reorganizations between room and cryogenic temperatures. These concern the radical units directly involved in intermolecular exchange interactions within the solid. The magnetic properties were found significantly altered. These observations address the question of the pertinence of a magneto−structural correlation based on crystal data obtained close to 293 K for intermolecular exchange interactions revealed for cryogenic temperatures.

Acknowledgment. This work was supported by King Fahd University of Petroleum and Minerals, Dhahran, Saudi Arabia, the CNRS, and the TMR Research Network ERBFMRXCT-980181 of the European Union, entitled "Molecular Magnetism, from Materials toward Devices".

Supporting Information Available: Six X-ray crystallographic files, in CIF format. This material is available free of charge via Internet at http://pubs.acs.org.

IC020021P